IEEE Access
Multidisciplinary ⋮ Rapid Review ⋮ Open Access Journal

Received 21 November 2024, accepted 3 December 2024, date of publication 9 December 2024, date of current version 20 December 2024.

Digital Object Identifier 10.1109/ACCESS.2024.3514162

RESEARCH ARTICLE

Traffic Signal Optimization in Large-Scale Urban Road Networks: An Adaptive-Predictive Controller Using Ising Models

DAISUKE INOUE[1,*], HIROSHI YAMASHITA[2,3,*], KAZUYUKI AIHARA[2], AND HIROAKI YOSHIDA[1]

[1]Toyota Central Research and Development Labs., Inc., Nagakute, Aichi 480-1192, Japan
[2]International Research Center for Neurointelligence, The University of Tokyo, Bunkyo, Tokyo 113-0033, Japan
[3]Graduate School of Information Science and Technology, Osaka University, Suita, Osaka 565-0871, Japan

Corresponding authors: Daisuke Inoue (daisuke-inoue@mosk.tytlabs.co.jp) and Hiroshi Yamashita (h.yamashita@ist.osaka-u.ac.jp)

This work was supported in part by the Intelligent Mobility Society Design, Social Cooperation Program, a Social Cooperation Research Program of Toyota Central Research and Development Labs., Inc.; and in part by The University of Tokyo.

*Daisuke Inoue and Hiroshi Yamashita contributed equally to this work.

ABSTRACT Realizing smooth traffic flow is important for achieving carbon neutrality. Adaptive traffic signal control, which considers traffic conditions, has thus attracted attention. However, it is difficult to ensure optimal vehicle flow throughout a large city using existing control methods because of their heavy computational load. Here, we propose a control method called AMPIC (Adaptive Model Predictive Ising Controller) that guarantees both scalability and optimality. The proposed method employs model predictive control to solve an optimal control problem at each control interval with explicit consideration of a predictive model of vehicle flow. This optimal control problem is transformed into a combinatorial optimization problem with binary variables that is equivalent to the Ising problem. This transformation allows us to use Ising solvers, which have been widely studied and are expected to offer fast and efficient optimization performance. The method works adaptively according to traffic conditions such as the structure of the road network and feedback from observation of the traffic system. We performed numerical experiments using a microscopic traffic simulator for a realistic city road network. Compared to the classical pattern control method, the results show that AMPIC increases the vehicle cruising speed by 13%, reduces the waiting vehicle ratio to 60%, and lowers the CO_2 emissions to only 25% of the original level. The model predictive approach with a long prediction horizon thus effectively improves control performance. Systematic parametric studies on model cities indicate that the proposed method realizes smoother traffic flows for large city road networks. Among Ising solvers, D-Wave's quantum annealing is shown to find near-optimal solutions at a reasonable computational cost.

INDEX TERMS Traffic control, quantum annealing, model predictive control.

I. INTRODUCTION

With global economic growth, urban traffic volumes have steadily increased. Addressing traffic congestion is essential for mitigating economic losses [1], ensuring driver well-being [2], and reducing carbon emissions [3]. In particular, the serious impact of CO_2 emissions on global temperatures, which has been confirmed by both climate models and measurement data, requires immediate action [4], [5], [6]. Efficient management and operation of traffic signals are essential for facilitating smooth traffic flow [7], [8], [9]. Traditionally, signal parameters such as cycle length, green time, and the change interval have been determined using statistical information based on observed traffic data [10], [11]. Recently developed intelligent traffic systems allow the acquisition of real-time traffic information [12], [13], enabling adaptive control that dynamically determines signal

The associate editor coordinating the review of this manuscript and approving it for publication was Yilun Shang.

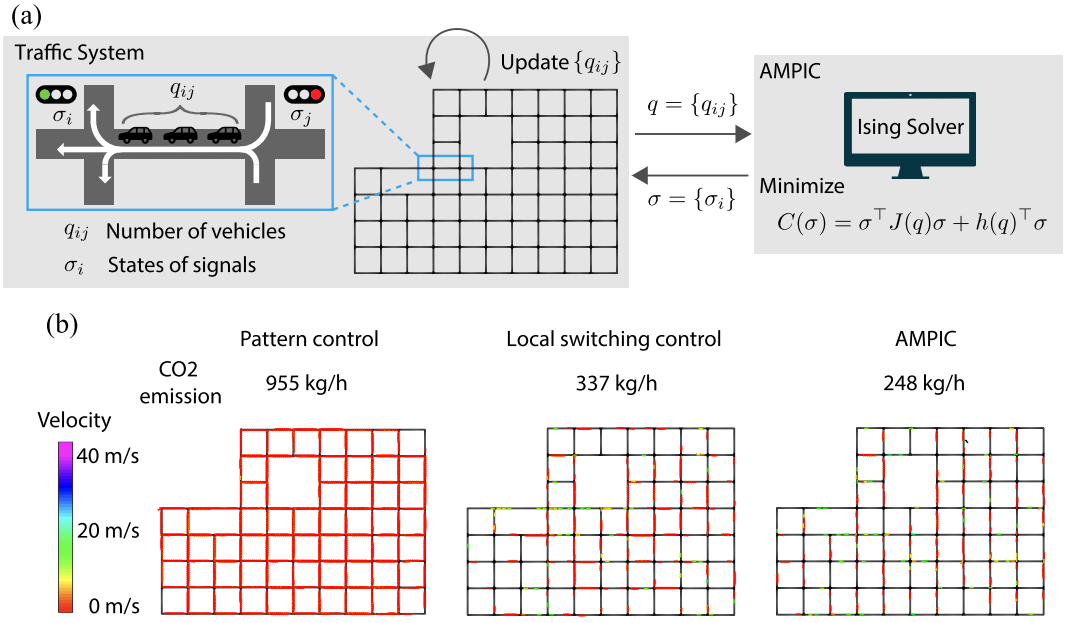

FIGURE 1. Schematic diagram of the proposed method (AMPIC) and snapshots of vehicles in SUMO with various traffic control methods. (a) Vehicle information collected from the traffic system is sent to AMPIC and control quantities computed by AMPIC are sent to traffic system (see Section III for explanation of variables). (b) Snapshots of vehicles in numerical evaluation with SUMO on roads that replicate urban areas in Sapporo, Hokkaido, Japan. The vehicle generation rate was set to 2.22 vehicles per second. The snapshots represent the state of vehicles 1 hour after the start of the simulation. The color of a vehicle represents its speed. The results for traditional pattern control, local switching control, and control with AMPIC are shown. The total CO_2 emissions for each control method are also shown.

states based on current traffic conditions [14], [15], [16], [17], [18], [19], [20]. Various approaches have been proposed to realize adaptive control, including heuristic optimization methods such as genetic algorithms [21], [22], [23], [24], evolutionary computation [25], [26], [27], and metaheuristic optimization [28], [29], [30], as well as artificial intelligence models such as neural networks and reinforcement learning [31], [32], [33], [34], [35]. These methods are particularly effective for urban traffic networks with rapidly changing traffic patterns [18]. However, the computational complexity of simultaneously determining multiple control variables and model parameters restricts their use to networks with only a few intersections. Decentralized control approaches, which divide the traffic model and the signal controller, have been proposed [36], [37], [38], but the information available for control is limited to the local neighborhood, preventing global optimization throughout an entire city. Therefore, the development of an algorithm that simultaneously and optimally determines control variables for large cities with many intersections remains an important challenge [7], [39].

Recently, methods using Ising models have gained attention as efficient approaches for solving large-scale combinatorial optimization problems. An Ising model, originally from statistical physics, describes the relation between the microscopic state of a spin system and the macroscopic phenomena of magnetic phase transitions [40], [41]. This model is equivalently convertible to a combinatorial optimization problem with binary variables, which includes various practical engineering problems such as delivery planning, packing, and the traveling salesman problem [42], [43]. Specialized solvers, known as Ising solvers, have been developed to find the ground state of the Ising model [44], [45], [46]. These solvers exploit the phenomenon of physical quantities reaching a stationary point in the search for a solution, which is expected to deliver higher performance than conventional Neumann-type computers. In particular, quantum annealing, which uses quantum fluctuations to search for the optimal solution, has attracted much attention since D-Wave Systems Inc. provided a commercially available solver. Its performance has been evaluated for various engineering problems [47], [48], [49], [50], [51], [52], [53], [54], [55].

In this paper, we propose a method that achieves both globally optimized traffic signal patterns and flexible adaptation to a large-scale road network and observed traffic conditions. To simultaneously determine the states of many traffic signals, we formulate an optimization problem that can be solved by Ising solvers. The proposed method is called AMPIC (Adaptive Model Predictive Ising Controller). The main contributions of this study are summarized by the following three aspects in which the proposed method is adaptive to the traffic conditions:

- It works adaptively according to *large-scale* traffic conditions. It employs Ising solvers to determine the traffic signal state at each time step. The optimization problem of traffic signals using an internal model that predicts the flow dynamics of vehicles traveling on an arbitrary road network (with up to four-way

intersections) is shown to be equivalent to the Ising problem. This enables scalable traffic signal control, allowing simultaneous optimization of multiple signals in large road networks, and offers flexibility in selecting optimization methods.

- It works adaptively according to *real* traffic conditions. The parameters of the internal model used by the proposed control method are adaptively determined by the road network structure. The proposed model consists of a feedback loop between the controller and the traffic system, which reduces the modeling error (compared to the actual traffic flow), providing the controller with the flexibility to adapt to various traffic scenarios.
- It works adaptively according to *future* traffic conditions. It employs model predictive control (MPC). The controller's internal model is used to predict traffic conditions up to multiple control cycles ahead and minimize an objective function to improve future traffic conditions. This approach avoids short-sighted control and is expected to achieve advanced traffic management.

Theoretically, the formulation of the Ising problem used in the proposed controller is obtained by extending our previous study [56]. In that study, the network and traffic model considered were too simplified to be applicable to real traffic situations. In comparison, the proposed method is more adaptive to real traffic conditions and more far-sighted in terms of time, allowing it to be applied to a wider and more practical range of traffic situations.

In this study, the performance of AMPIC is systematically evaluated using an external microscopic traffic flow simulator, namely Simulation of Urban MObility (SUMO) [62], which is widely used to model realistic urban traffic (see Fig. 1). Performance is assessed using practical metrics such as waiting time and CO_2 emissions. The results show that AMPIC increases the vehicle's cruising speed and reduces waiting time compared to those obtained with conventional control methods, while also significantly lowering CO_2 emissions. Notably, the model predictive approach enhances control performance, particularly when an extended prediction horizon is employed. Parameter studies with model cities show that AMPIC achieves more efficient traffic flows than those obtained with other control protocols, especially for very large cities, indicating the need for global optimization that considers many intersections simultaneously. We also show that D-Wave's quantum annealing consistently finds near-optimal solutions at reasonable computational cost.

II. RELATED WORK

Several studies, including our previous work [56], have explored the connection between signal control problems and Ising-type models [57], [58], [59]. Hussain et al. [57] proposed a method for maximizing traffic flow in a lattice network by coordinating adjacent signals. Marchesin et al. [58] proposed an optimization problem for controlling groups of vehicles traveling on arbitrary road networks. Similarly, Shikanai et al. [59] designed an optimization problem to determine signal guidance modes for controlling groups of vehicles traveling on arbitrary road networks. Most of these studies, except [59], validated their controllers using coarse-grained macroscopic traffic simulations. In contrast, our approach is tested using detailed microscopic simulations where individual vehicles follow specific traffic rules. In addition, unlike [59], our method integrates MPC, which allows for more sophisticated signal management by predicting future traffic conditions. A comparison of these methods with our approach is provided in Table 1.

Apart from the Ising problem approach, several MPC approaches have been proposed for traffic signal control; they can be broadly classified as centralized, hierarchical, and distributed MPC [60]. In centralized MPC, a single controller collects information from the entire network and issues control commands, taking into account subsystem interactions [20], [63], [64], [65]. Although this method can achieve optimal network-wide coordination, it often faces computational challenges, particularly for large networks. Hierarchical MPC addresses this problem by dividing the network into layers, with higher-level controllers managing overall objectives and lower-level controllers handling local optimizations [66], [67]. This structure reduces computational complexity and improves scalability. Distributed MPC further decentralizes control by assigning tasks to independent subsystems that coordinate locally, making it well suited to large urban networks due to its relatively low computational load [68], [69], [70], [71]. Our approach falls into the category of centralized MPC. Although centralized MPC approaches are typically computationally intensive, we address this by using the Ising model and its solver to mitigate these challenges.

Regarding adaptive control methods other than MPC, heuristic algorithms are the most widely used due to their design flexibility. Among them, genetic algorithms have been extensively studied [21], [22], [23], [24]. Neural networks and reinforcement learning have also been studied for application to traffic signal systems thanks to advances in deep learning [31], [32], [33], [34], [35]. In the multi-agent approach, traffic signals at intersections are considered as agents. Often combined with reinforcement learning, they achieve coordinated signal control by cooperating or competing with each other to optimize signal display parameters [72], [73], [74], [75]. Research is also actively underway to achieve coordinated control in mixed autonomous vehicle environments [76], [77], [78], [79], [80]. For a broader explanation of these methods, we refer the reader to relevant survey papers [18], [61], [81], [82].

III. METHOD

A. OVERALL ALGORITHM

In this study, we consider the problem of controlling traffic signals in a road network with N intersections. We consider the graph $G = (V, E)$, where $V = \{1, \ldots, N\}$ denotes the

TABLE 1. Comparison with previous studies.

	[57]	[58]	[59]	Ours
Applicable Graph	Lattice	Arbitrary	Arbitrary	Arbitrary (up to 4-way intersection)
Model Predictive Control	No	No	No	Yes
Model for Validation	Macroscopic Model	Macroscopic Model	Microscopic Model	Microscopic Model

index of an intersection and E denotes the roads connecting to it. We assume that the network is directed. A road from intersection j to intersection i is denoted by (i, j). We consider up to four-way intersections (i.e., there are at most four roads leading to intersection i). The signal state at intersection i at time t, which represents the direction in which vehicles are allowed to proceed, is denoted by $\sigma_i(t) \in \{\pm 1\}$, and the number of vehicles on road (i, j) at time t is denoted by $q_{ij}(t)$. We assume that the signal state $\sigma_i(t)$ is determined at discrete time $t = \tau k$ ($k \in \mathbb{N}$) with a predetermined control cycle $\tau > 0$, and that once the signal is determined, the state $\sigma_i(t)$ is fixed until the next control cycle $\sigma_i(t + \tau)$.

Algorithm 1 Adaptive Model Predictive Ising Controller (AMPIC)

Input : $q_{ij}(t)$ ($(i, j) \in E$): Number of vehicles on each road
Output: $\sigma_i(t)$ ($i \in V$): Traffic signal states at each intersection
Identify difference equation (2) by using the number of vehicles $q(t)$.
Construct objective function $C(\sigma([t, \ldots, t + k_h]))$ in Eq. (3).
Convert the objective function to Ising model in (4).
Solve the Ising problem with Ising solver and obtain $\sigma^*([t, \ldots, t + k_h]) = \text{argmin } C(\sigma([t, \ldots, t + k_h]))$.
Return $\sigma^*(t)$.

As shown in Fig. 1a, the proposed system consists of a feedback loop between the controller and the traffic system. In each control cycle, AMPIC receives the number of vehicles $q_{ij}(t)$ from the traffic system and sends back the traffic signal states in the next control cycle. The controller first calculates the necessary parameters for constructing the objective function of the optimization problem. Then, the optimization problem is converted to an Ising problem. Finally, the Ising problem is solved by the Ising solver and the states of the signals $\sigma(t) := [\sigma_1(t)\, \sigma_2(t)\, \cdots\, \sigma_N(t)]^\top \in \mathbb{R}^N$ at the current time t are determined. The details of the algorithm are shown in Algorithm 1. The flowchart of the numerical simulation is shown in Fig. 2.

To simulate a traffic system, we used the open-source software SUMO [62], a microscopic traffic simulator. In the simulation, each vehicle travels through the city under realistic traffic conditions. In SUMO, vehicles travel along a preplanned route, whose origin and destination are randomly chosen. The position, speed, and other states of the vehicles

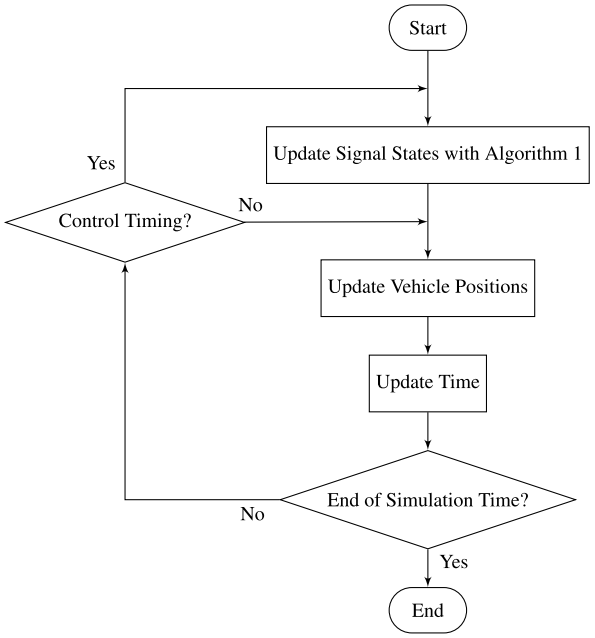

FIGURE 2. Flowchart of numerical simulations.

are updated sequentially at each time step (set to 1 second). The number of vehicles on roads q_{ij} is calculated and sent to AMPIC. In AMPIC, the Ising model is constructed using the values of q_{ij} and then the optimal states of all traffic signals are calculated. SUMO receives the signal states from AMPIC and updates the positions of all vehicles, changing the signal displays according to realistic procedures, such as inserting a yellow phase when the signal states change. Note that the calculation of control inputs does not necessarily require simulation with SUMO; it requires only the number of vehicles observed at each time step. See the Appendix for the detailed simulation procedures.

B. MODEL PREDICTIVE CONTROL OF TRAFFIC SIGNALS

Here, we describe the procedure for constructing the time evolution equation and the objective function necessary to formulate the MPC problem.

First, based on the traffic signal states and road positioning, we introduce the variable $s_{ij} \in \{\pm 1\}$. If the traffic light at intersection i with the state σ_i indicates green for the road (i, j), we assign the state value σ_i to s_{ij}. Then, the traffic light indicates green for the road (i, j) when $\sigma_i s_{ij} = +1$ and red when $\sigma_i s_{ij} = -1$. The definitions of these symbols are shown in Fig. 3. Depending on the indication of the traffic

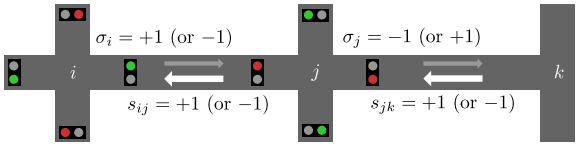

FIGURE 3. Definition of variables for road networks.

light, the roads leading to the intersection are classified as being on the red side or the green side. As in our previous study [56], we control the traffic system such that vehicles entering the intersection are equally distributed on these two sides. In particular, we define vehicle bias x_i at intersection i to represent how the situation differs from such condition:

$$x_i(t) := \sum_{j \in N_i} \eta_{ij} s_{ij} q_{ij}(t), \tag{1}$$

where N_i is the set of intersection indices that have a road leading to intersection i. In a typical example of east-west and north-south road intersections, x_i represents the difference between the number of vehicles present in the east-west direction and that in the north-south direction. In contrast, in this study, we incorporate the parameter $\eta_{ij} > 0$ to adapt to the condition of the road network. This parameter normalizes the different road lengths in the network and accounts for three-way intersections.

The traffic signal states at each time step are determined based on the feedback from the observation of the traffic system. We employ MPC, namely, the traffic signal pattern is determined by the controller based on the predicted traffic states from the observed current state. To predict the future traffic state, we use a simple linear model, assuming that the changes in the number of vehicles $q(t)$ are constant given the traffic light pattern σ within the prediction horizon. Then, the bias is expressed by the following linear difference equation:

$$x(t + \tau) = x(t) + \tilde{A}\sigma(t) + \tilde{b}, \tag{2}$$

where the vector $x(t) := [x_1(t)\ x_2(t)\ \cdots\ x_N(t)]^\top \in \mathbb{R}^N$ denote the vector of the vehicle bias.

The matrix $\tilde{A}$ and the vector $\tilde{b}$, that depend on the conditions of the road network, are computed with the estimated outflow rate and turn probabilities of vehicles. Further model details, such as the parameter η_{ij} in Eq. (1) and the forms of $\tilde{A}$ and $\tilde{b}$ in Eq. (2) are given in the Appendix.

We use the following objective function for MPC:

$$C(\sigma([t, \ldots, t + (k_\mathrm{h} - 1)\tau])) = \sum_{k=1}^{k_\mathrm{h}} x(t + k\tau)^\top Q x(t + k\tau), \tag{3}$$

where $k_\mathrm{h} \in \mathbb{N}$ is a constant called the prediction horizon; a large value of k_h takes into account a long-term future. The diagonal matrix $Q \in \mathbb{R}^{N \times N}$ is used to set the relative weight of importance on the intersections; $Q = I_N$, where I_N denotes the N-dimensional identity matrix, means that all intersections are equally important. Equation (3) aggregates the vehicle bias for every intersection at each time step. By minimizing this quantity, we expect to eliminate the uneven flow of vehicles throughout the city, resulting in smooth, congestion-free traffic flow.

C. TRANSFORMING MPC INTO ISING PROBLEM

Here, we describe the method used for transforming the formulated MPC problem into an Ising problem. The Ising problem derived in this study takes the following form:

$$\underset{\boldsymbol{\sigma}(t)}{\text{minimize}} \sum_{i<j} J_{ij}\boldsymbol{\sigma}_i(t)\boldsymbol{\sigma}_j(t) + \sum_i h_i\boldsymbol{\sigma}_i(t), \tag{4}$$

where we consider Nk_h decision variables, denoted by $\boldsymbol{\sigma} \in \{\pm 1\}^{Nk_\mathrm{h}}$, and consider $J \in \mathbb{R}^{Nk_\mathrm{h} \times Nk_\mathrm{h}}$ and $h \in \mathbb{R}^{Nk_\mathrm{h}}$ as the parameters that characterize this problem. These variables and the objective function correspond to the spin variables and energy of the Ising model, respectively.

The Ising problem is both an engineering optimization problem and a physical model. Researchers have thus attempted to utilize the model as a solver for optimization problems by constructing a physical system or hardware that minimizes Eq. (4) (see, for example, [44], [45], [46]). In this study, these solvers are referred to as Ising solvers. Examples of such hardware include coherent Ising machines [46], [83], simulated bifurcation machines [45], digital annealers [84], [85], and quantum annealing machines from D-Wave Systems Inc. [44], [86]. Among these, quantum annealing machines have attracted attention as a non-von Neumann, commercially available computer architecture that takes advantage of quantum fluctuations. Their applications are currently under investigation [49], [87], [88], [89], [90], [91], [92]. By inputting the coefficients J and h of the Ising problem, these solvers output $\boldsymbol{\sigma}^*$, the minimizer of the energy of the Ising model. Although the performance varies among Ising solvers, it should be noted that the proposed method can be implemented using any of these solvers.

Following standard procedures, it is possible to transform the MPC problem into the Ising problem in Eq. (4). First, by stacking σ and x along the time axis, we construct the following extended variables:

$$\boldsymbol{\sigma}(t) = [\sigma(t)^\top \cdots \sigma(t + (k_\mathrm{h} - 1)\tau)^\top]^\top \in \{\pm 1\}^{Nk_\mathrm{h}}, \tag{5}$$

$$\mathbf{x}(t) = [x(t)^\top \cdots x(t + (k_\mathrm{h} - 1)\tau)^\top]^\top \in \mathbb{R}^{Nk_\mathrm{h}}. \tag{6}$$

We also define the matrices $\mathbf{I}$, $\mathbf{A}$ and the vector $\mathbf{b}$ as follows:

$$\mathbf{I} = \begin{bmatrix} I_N & I_N & \cdots & I_N \end{bmatrix}^\top \in \mathbb{R}^{Nk_\mathrm{h} \times N}, \tag{7}$$

$$\mathbf{A} = \begin{bmatrix} \tilde{A} & 0 & \cdots & \cdots & 0 \\ \tilde{A} & \tilde{A} & \ddots & & \vdots \\ \vdots & \ddots & \ddots & \ddots & \vdots \\ \tilde{A} & \tilde{A} & \cdots & \tilde{A} & 0 \\ \tilde{A} & \tilde{A} & \cdots & \tilde{A} & \tilde{A} \end{bmatrix} \in \mathbb{R}^{Nk_\mathrm{h} \times Nk_\mathrm{h}}, \tag{8}$$

$$\mathbf{b} = \begin{bmatrix} \tilde{b}^\top & 2\tilde{b}^\top & \cdots & k_\mathrm{h}\tilde{b}^\top \end{bmatrix}^\top \in \mathbb{R}^{Nk_\mathrm{h}}. \tag{9}$$

By using Eq. (2), we obtain the following equality:

$$\mathbf{x}(t+\tau) = \mathbf{I}x(t) + \mathbf{A}\boldsymbol{\sigma}(t) + \mathbf{b}. \tag{10}$$

Using this, Eq. (3) is rewritten as follows:

$$\begin{aligned} &C(\sigma([t,\ldots,t+(k_\mathrm{h}-1)\tau])) \\ &\quad = \mathbf{x}(t+\tau)^\top \mathbf{Q}\,\mathbf{x}(t+\tau) \\ &\quad = [\mathbf{I}x(t) + \mathbf{A}\boldsymbol{\sigma}(t) + \mathbf{b}]^\top \mathbf{Q}\,[\mathbf{I}x(t) + \mathbf{A}\boldsymbol{\sigma}(t) + \mathbf{b}] \\ &\quad = \boldsymbol{\sigma}(t)^\top \mathbf{A}^\top \mathbf{Q}\mathbf{A}\boldsymbol{\sigma}(t) + 2[\mathbf{I}x(t) + \mathbf{b}]^\top \mathbf{Q}\mathbf{A}\boldsymbol{\sigma}(t) + \boldsymbol{c}, \end{aligned} \tag{11}$$

where $\mathbf{Q}$ is the block diagonal matrix $\mathbf{Q} := \mathrm{diag}\{Q,\ldots,Q\}$ and $\boldsymbol{c} := [\mathbf{I}x(t) + \mathbf{b}]^\top \mathbf{Q}[\mathbf{I}x(t) + \mathbf{b}]$. Equation (11) is the form of the Ising model of Eq. (4).

It is not always possible to convert optimization problems to the Ising problem. In our previous study [56], a method for representing the traffic signal control problem as an Ising problem was proposed and its conceptual effectiveness in large-scale networks was demonstrated. However, the network and traffic model considered in that study were highly simplified and the applicability to more realistic road networks was not fully investigated. The novelty of the present study lies in demonstrating that the conversion of a broader class of traffic signal control problems to an Ising problem is feasible.

IV. RESULTS

A. EVALUATION CRITERIA

The objective function (3) used in the proposed method does not directly correspond to the conventional evaluation criteria for traffic conditions. Thus, the performance of the proposed controller is compared with that of existing methods using the following performance indicators:

- Mean velocity: the average speed of all vehicles in the road network.
- Waiting vehicle ratio: the ratio of the number of stopped vehicles to the number of all vehicles in the road network. Here, vehicles moving at a speed below 0.1 m/s are counted as stopped vehicles.
- CO_2 emissions: the total amount of carbon dioxide emitted by all vehicles on the road per time step, which is computed using a model included in SUMO [93].
- Sum of squared vehicle bias: the value of the objective function defined in Eq. (3), evaluated at each time step using the obtained $\sigma(t)$:

$$\tilde{C}(t) = x(t)^\top Q x(t). \tag{12}$$

Among these, the first indicator is considered more desirable when its value is higher, while the remaining three indicators are more desirable when their values are lower. In addition, the first three performance indicators directly evaluate the desirability of traffic conditions and the last performance indicator is closely related to the minimized objective function (i.e., the Ising model). We compare the proposed method with the following control methods:

- Local switching control [94]: This controller greedily reduces the vehicle bias for each intersection, considering only the local vehicle bias rather than minimizing a global objective function. The state of signal σ_i at each intersection i is defined as

$$\begin{cases} \sigma_i(t) \leftarrow +1 & \text{if } x_i(t) > 0, \\ \sigma_i(t) \leftarrow \sigma_i(t-\tau) & \text{if } x_i(t) = 0, \\ \sigma_i(t) \leftarrow -1 & \text{if } x_i(t) < 0. \end{cases} \tag{13}$$

- Random control: This control method switches the state of each signal with a certain probability at each control cycle. The switching probability per control cycle is assumed to be 0.5.
- Pattern control: This control method switches the state of the signal at each predetermined control cycle. The switching cycle is assumed to be once every two control cycles for compatibility with random control. Here, two types of patterns for the initial states are considered:
  - Random pattern: The initial display of the traffic signals is set randomly.
  - Coordinated pattern: Initially, the same color is displayed for all signals in the same direction.

Of the methods mentioned above, random and pattern control are not adaptive control methods because they do not determine signal displays based on traffic conditions. Among pattern controls, the coordinated pattern is the simplest coordinated traffic signal control. Local switching control, while a basic adaptive control method, sets the signals at each intersection independently; it lacks a mechanism to coordinate neighboring signals. In contrast, the proposed method determines signal displays for the entire city by solving an optimization problem that allows for potential coordination between adjacent signals.

The vehicle origin location, destination, and routing follow SUMO's default settings (see the Appendix for details). Unless otherwise noted, the parameters of the controller are defined as follows: the control period is $\tau = 60$ s, the prediction horizon is $k_\mathrm{h} = 1$, and the weight matrix is $Q \equiv I_N$. For the Ising solver, we use *SimulatedAnnealingSampler* [95] provided by D-Wave Systems and set the parameter *num_reads* to 1000. For the other hyperparameters in the solver, the default values are used.

B. RESULTS FOR SAPPORO ROAD NETWORK

We created a road network that corresponds to an urban area in Sapporo, Japan, as shown in Fig. 4. In this road network, we assumed that all intersections have traffic signals. The time evolution of the mean velocity, waiting vehicle ratio, CO_2 emissions, and sum of squared vehicle bias are shown in Fig. 5. The number of vehicles added to the road network per time step, which we refer to as the vehicle generation rate, is set to 2.22 vehicles per second. The figure shows the average value over five simulation runs in which the vehicles had different routes. For legibility, the 120-second moving average for each performance indicator is shown.

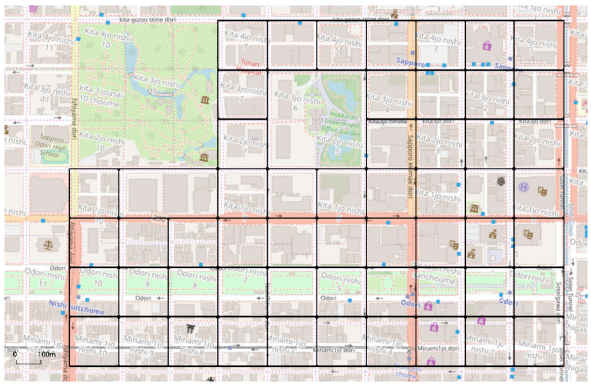

FIGURE 4. Road network created to replicate urban area of Sapporo, Hokkaido, Japan. The base map image is provided by ©OpenStreetMap [96], [97], [98].

As shown in Figs. 5a and 5b, with the non-adaptive methods (i.e., random and pattern control methods), the mean velocity decreases over time and the waiting vehicle ratio approaches 1, indicating that congestion occurs. The congestion results in an increasing number of vehicles in the network. Consequently, the CO_2 emissions increase steadily, as shown in Fig. 5c. Coordinated pattern control has slightly better performance than random pattern control. In contrast, with local switching control and the proposed control method, the mean velocity and waiting vehicle ratio approach a steady state after a short initial transient response. This results in low CO_2 emissions due to the balance between the number of vehicles that are added and the number of vehicles that are removed (i.e., vehicles that reach their destinations). The proposed control method achieves a shorter waiting time and a faster cruising speed than those obtained with local switching control. The CO_2 emissions are accordingly lower. In Fig. 5d, the proposed method shows the lowest vehicle bias among all methods. This is expected as this performance indicator is directly minimized in the proposed method, but not in the other methods.

We next examine situations with different numbers of vehicles. Simulations were performed with various vehicle generation rates. Figure 6 shows the time-averaged values of the mean velocity, waiting vehicle ratio, CO_2 emissions, and sum of squared vehicle bias as functions of the vehicle generation rate. For each simulation run, the value of a given performance indicator was averaged in time over 3600 seconds. Each data point and error bar indicate the mean value and standard error, respectively, for five simulation runs with different vehicle routes.

Figures 6a and 6b show that in general, an increase in the vehicle generation rate leads to a lower average speed and more stopped vehicles. The proposed method mitigates the decrease in mean velocity and thus the waiting vehicle ratio and the CO_2 emissions are suppressed. Local switching control shows performance similar to that of the proposed method, but the degradation of traffic conditions occurs at a smaller vehicle generation rate than that for the proposed method. Among the non-adaptive methods, coordinated pattern control gives the best results, but it is inferior to the proposed method and local switching control. At the maximum generation rate in our experiment, the performance difference between the methods disappears, indicating that congestion is unavoidable. Similar trends were found for CO_2 emissions, as shown in Fig. 6c, suggesting that better traffic conditions are also beneficial for decarbonization. As shown in Fig. 6d, the proposed method minimizes the energy of the Ising model the most for all vehicle generation rates. This result confirms the correspondence between the performance indicator defined via vehicle bias and other performance indicators (velocity, waiting vehicle ratio, and CO_2 emissions). We calculated the average queue length of vehicles near the intersection as another index of traffic flow. The result showed a similar trend to the other indices above.

C. EFFECT OF ROAD NETWORK SIZE

We now examine the performance of the proposed method for road networks with various sizes. Here, we use square lattice networks that consist of N intersections, with N varied from 5×5 to 25×25. The distance between adjacent intersections is fixed at 100 m. Since local switching control was found to be the most comparable method in the previous subsection, it is used here for comparison with AMPIC.

Figure 7 compares the performance of the proposed global control method and local switching control for various vehicle generation rates. For precision, the horizontal axis is the scaled vehicle generation rate $\tilde{p}$, which is defined as the vehicle generation rate divided by $\sqrt{N}$. This was done because the average distance traveled by an individual vehicle scales as $O(\sqrt{N})$, and thus so does the average time t_{av} for which a vehicle remains in the network. In addition, the total road length L_{total} of the network scales as $O(N)$. Therefore, the average density of vehicles in the road network is estimated as $p \times t_{av}/L_{total} \sim p/\sqrt{N}$, where p is the vehicle generation rate. This horizontal axis enables us to compare the results for different network sizes. For example, both the mean velocity and the waiting vehicle ratio exhibit universal sudden changes of behavior around $\tilde{p} \sim 0.3$. Figures 7d-f plot the results of AMPIC relative to those of the local switching control. Since in the region $\tilde{p} < 0.3$ the relative velocity is above unity and the relative waiting vehicle ratio is below unity, AMPIC results in a faster vehicle cruising speed and a lower number of stopped vehicles than those obtained with local switching control. The performance difference becomes very large for $\tilde{p} \approx 0.4$ (because congestion occurs only for local switching control). For high vehicle generation rates ($\tilde{p} > 0.5$), the relative performance difference between the two methods disappears, as in the previous section.

The relative performance difference between the proposed method and the local switching control is larger when the network size is increased, especially in the region of $\tilde{p} < 0.3$. This result suggests the global nature of many-body traffic systems that have long-range correlations and the importance of traffic signal optimization that simultaneously

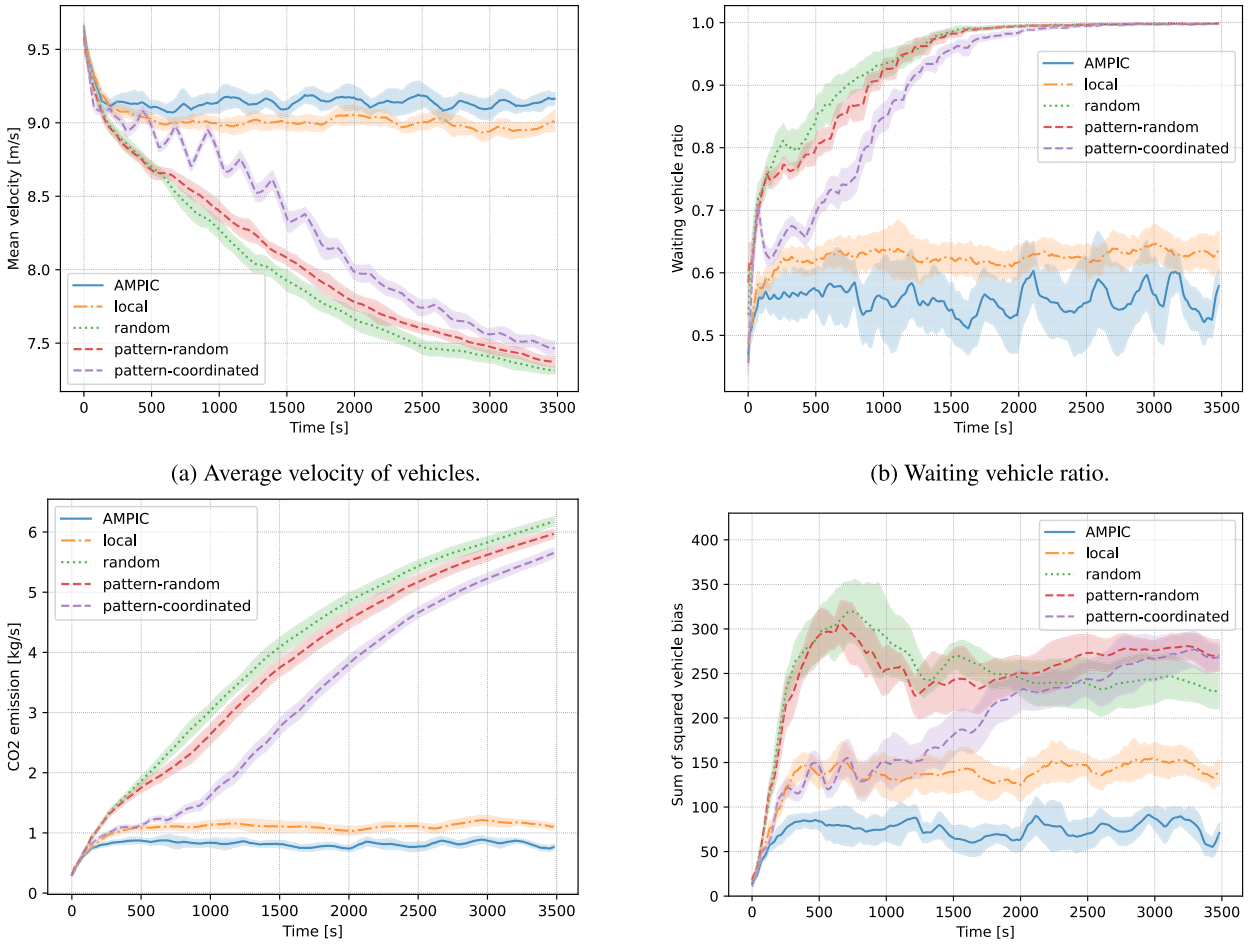

(a) Average velocity of vehicles.

(b) Waiting vehicle ratio.

(c) CO_2 emissions.

(d) Sum of squared vehicle bias.

FIGURE 5. **Time evolution of performance indicators for various methods. The proposed method (blue solid) is compared with local switching control (orange dash-dotted), random control (green dotted), random pattern control (red dashed), and coordinated pattern control (purple dashed). The colored area represents the standard error of each performance indicator for various seeds of the random number used for vehicle route generation.**

considers distant intersections. In addition, in Figs. 6 and 7, the observed shifts from a smooth traffic state to a congested state are sharp. We also observed a large fluctuation (or sample variance, as shown by the error bars) around the transition point. Such observations can be interpreted as global phenomena such as bifurcations or phase transitions of the spin system. This also supports the importance of optimizing the overall traffic signal pattern in the system. Similar to the results for the waiting vehicle ratio, the CO_2 emissions are greatly reduced with the proposed method, especially for a large network.

D. EFFECT OF PREDICTION HORIZON

We next examine the effect of the prediction horizon k_h on control performance. Here, we use a lattice network with $N = 10 \times 10$, with the value of k_h varied from 1 to 10. The results are plotted in Fig. 8. As the prediction horizon is extended, the mean velocity increases and the waiting vehicle ratio tends to decrease, resulting in a decrease in CO_2 emissions. The slight improvement observed for a horizon longer than six steps indicates the limitation of the model prediction. Given that the control cycle is 60 seconds, this result suggests that considering prediction horizons longer than 6 minutes does not significantly improve traffic conditions. This limitation may result from the relatively low prediction accuracy for a long horizon, the degradation of optimization performance for a large optimization problem, or both.

E. EFFECT OF ISING SOLVER

AMPIC is compatible with all Ising solvers, including those based on quantum annealing. The effect of the solver on performance is of interest not only for the implementation of traffic signal control but also for Ising solver development. Thus, we compare the results obtained with various Ising solvers for a lattice network with $N = 10 \times 10$. The following three solvers are used (refer to the Appendix for detailed solver settings):

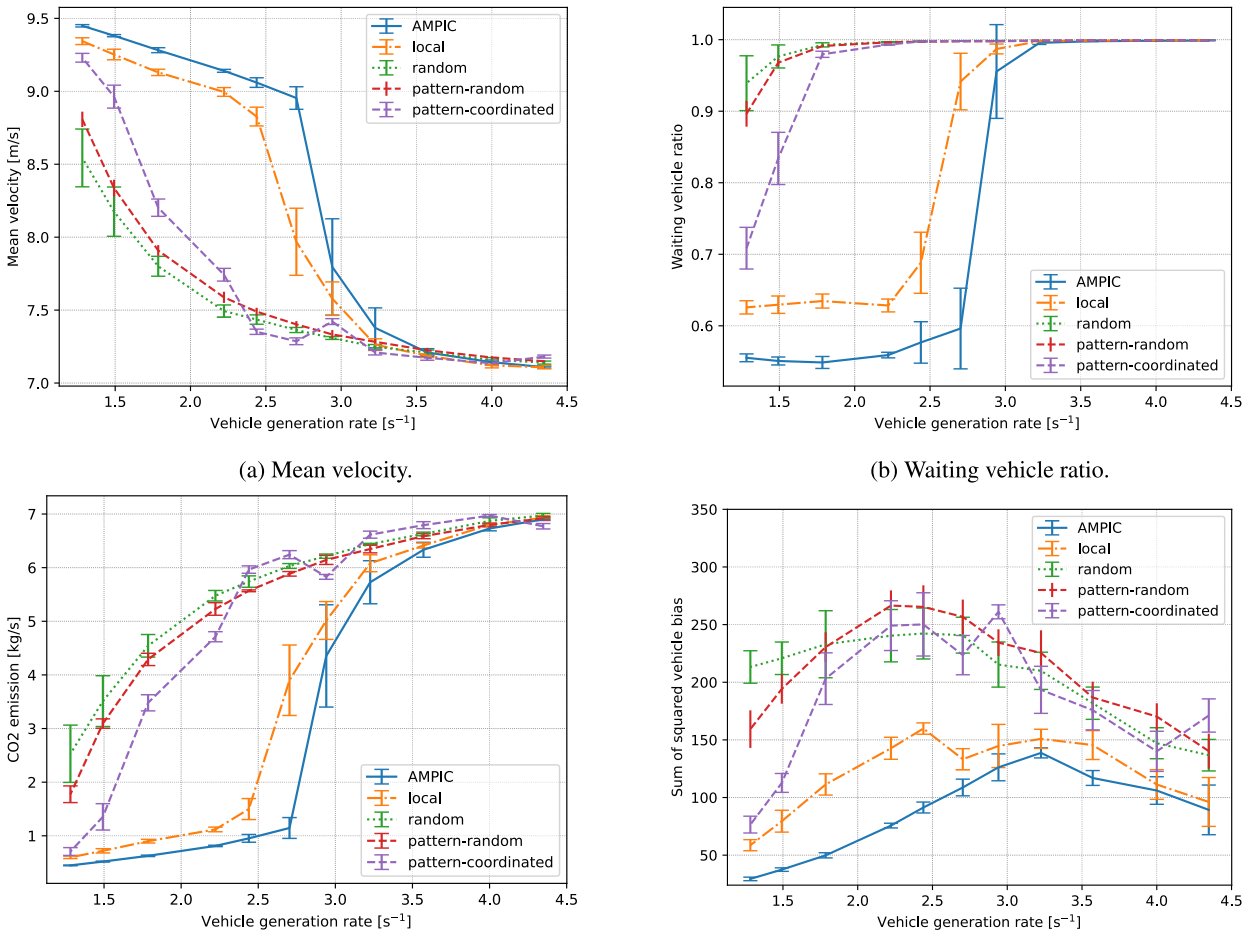

(a) Mean velocity.

(b) Waiting vehicle ratio.

(c) CO_2 emissions.

(d) Sum of squared vehicle bias.

FIGURE 6. **Time-averaged performance indicators for various vehicle generation rates for various methods. The proposed method (blue solid) is compared with local switching control (orange dash-dotted), random control (green dotted), random pattern control (red dashed), and coordinated pattern control (purple dashed). The error bars represent the standard error of each performance indicator for various seeds of the random number used for vehicle route generation.**

- Greedy method: This method is regarded as a discrete analog of the gradient descent method for continuous functions. At each step, the state obtained by flipping the variable that produces the highest energy decay is chosen as the next state.
- Simulated annealing (SA): This algorithm searches for the solution by repeatedly transitioning to the next state in a random neighborhood of the current solution. The selection is guided by a parameter called the temperature, which is progressively reduced with each iteration of the update. This feature reduces the possibility of the solution falling into a local minimum.
- Quantum annealing (QA): This algorithm is regarded as a quantum version of SA. Quantum annealing uses quantum fluctuation to simultaneously search for candidate solutions to find the global minimum of the objective function. This is expected to enable faster and more accurate solution searches than those of non-quantum methods.

The results are shown in Table 2. The performance of SA and QA is much better than that of the greedy method. In particular, the CO_2 emissions for the greedy method are more than 25% higher than those for SA and QA. The emissions for QA are slightly higher than those for SA, but the time required to solve the problem with QA is much shorter than that for SA. Note that these results depend on the computational environment. Using a high-performance CPU for SA will shorten the computation time. Note that the computation time for the quantum annealing method was measured in terms of *qpu_access_time* [99], which excludes the communication time between Canada (where the D-Wave machine is installed) and Japan (where the experiment was conducted) and the waiting time for the start of processing. In our simulations, the control cycle was set to 60 seconds and all solvers compared here completed their computations within this time frame. To respond to sudden changes in traffic conditions, however, it is preferable to be able to set a shorter control cycle. Given the trade-off between

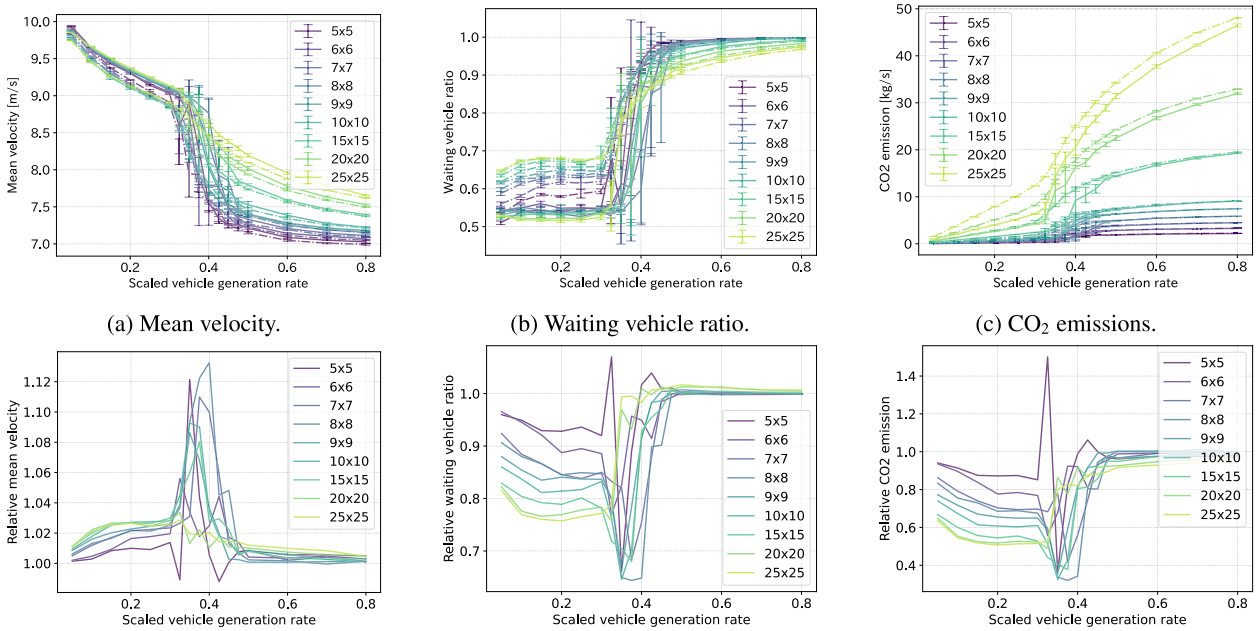

(a) Mean velocity. (b) Waiting vehicle ratio. (c) CO_2 emissions.

(d) Relative mean velocity. (e) Relative waiting vehicle ratio. (f) Relative CO_2 emissions.

FIGURE 7. Time-averaged performance indicators for various city sizes and vehicle generation rates. Top and bottom panels show absolute and relative values, respectively. In the top panel, solid lines show the results of AMPIC and dashed lines show the results of local switching control.

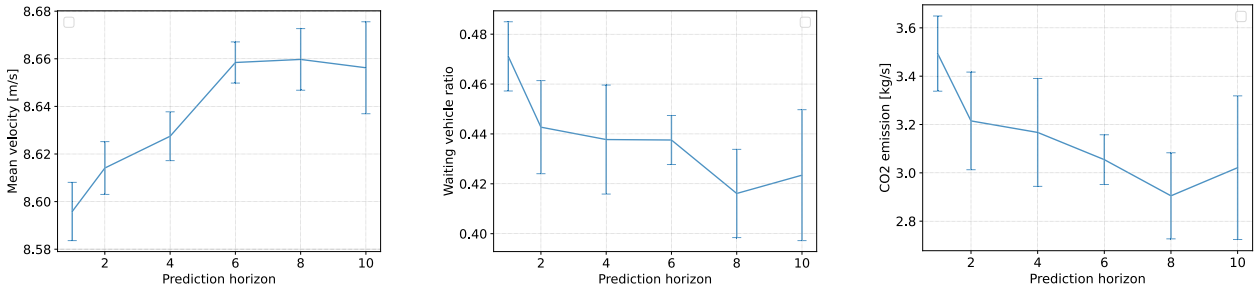

(a) Mean velocity. (b) Waiting vehicle ratio. (c) CO_2 emissions.

FIGURE 8. Time-averaged performance indicators for various prediction horizons. The error bars represent the standard errors of each performance indicator for various seeds of the random number used for vehicle route generation.

TABLE 2. Time-averaged performance indicators for control implemented with various Ising solvers.

	Greedy	SA	QA
Mean velocity [m/s]	8.669 ± 0.056	8.749 ± 0.058	8.739 ± 0.056
Waiting vehicle ratio	0.576 ± 0.025	0.485 ± 0.024	0.504 ± 0.025
CO_2 emissions [kg/s]	3.617 ± 0.224	2.722 ± 0.110	2.876 ± 0.121
Sum of squared vehicle bias	93.051 ± 7.252	56.999 ± 4.170	68.776 ± 5.388
Elapsed time [s]	$0.031 \pm 4.64 \times 10^{-4}$	1.866 ± 0.168	$0.561 \pm 3.42 \times 10^{-2}$

performance and time, a quantum annealing machine is a practical candidate for the optimization solver in the situation considered in the present study.

Apart from the solvers compared above, benchmarks have been performed using a variety of general optimization problems [100], [101]. The performance of each solver depends on the form of the Ising problem. Comparing the performance of solvers other than those considered in this study remains a task for future work. In addition, in high-performance computing for large-scale problems, it is important to reduce the energy consumption of the computing system itself [102]. One of the advantages of Ising solvers is their ability to solve problems with high energy efficiency [103]. The evaluation of methods, including in terms of the

CO_2 emissions from the optimization process itself, for the problem addressed in this study remains a task for future work.

V. CONCLUSION

We showed that the model predictive control of traffic signals achieved by solving the Ising problem significantly reduces traffic congestion and therefore decreases CO_2 emissions. The MPC was shown to work appropriately for various prediction lengths (see Fig. 8). The observed improvement compared to the local switching control was greater for a larger traffic network (see Fig. 7), which supports the importance of simultaneously considering all distant traffic signals for a road network that may have long-range correlations. Furthermore, the D-Wave machine was found to provide near-optimal solutions in a short time (see Table 2).

Here, the sudden shift from a smooth traffic state to a congested state (see Fig. 7) and the large fluctuation (or sample variance shown by error bars) around the transition point can be considered phase transitions. However, the distinction between the two phases is sharper for small networks, which is opposite to the general trend for phase-transition phenomena. This difference could be the result of the intervention of signal control, which acts to blur the phase transition, resulting in smooth traffic states. A detailed discussion of this transition phenomenon and an investigation of finite-size scaling for the present system will be presented in future studies.

In the proposed method, we used a simple linear traffic model in the controller that assumes a constant flow rate in each time interval. This model may be inaccurate compared to more complex traffic models, such as those that consider the saturation of neighboring roads [38]. We emphasize that our control approach, despite using a simple traffic model, still achieves global optimization and improves the traffic situation in large networks, which is achieved by the centralized nature of the proposed method.

In addition, formulating the problem as an Ising problem will allow us to take advantage of future advances in Ising solvers, such as quantum computers, with minimal development costs (solvers can simply be plugged into the controller). As a result of simplification, our model considers only two signal states for each intersection. In future research, we plan to extend the model to more complicated situations by handling more than two signal states or by incorporating state variables not included in the current model, such as occupancy and density.

In this study, the evaluation was performed using a widely used realistic microscopic traffic flow simulator (SUMO) [62]. For practical implementation, it will be necessary to install some devices at each intersection to provide important information for the control method (i.e., the values of x_i in Eq. (1)). To enable this, methods such as installing cameras at intersections or using vehicle-to-infrastructure communication to transmit vehicle positions obtained via GPS can be considered [12], [13]. A robust communication network is required for sending the observed vehicle information to the Ising solver and receiving control commands without delay or data loss. Verification of the computational reliability of the Ising solver is also critical. Careful validation of these factors will be important for the practical application of the proposed method.

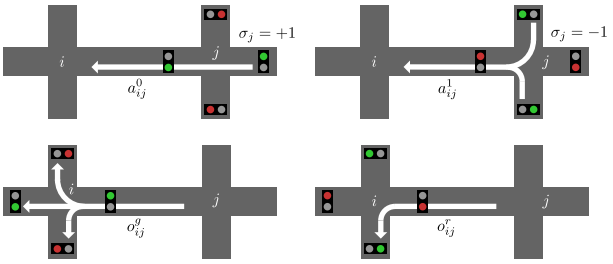

FIGURE 9. Illustration of vehicle flowrates in road networks.

APPENDIX

CONSTRUCTION OF TIME EVOLUTION EQUATION

Here, we describe the method used for constructing the time evolution equation shown in Eq. (2). We first consider the vehicle flow rate at which the cars enter road (i, j) through intersection j per unit time. Let a^0_{ij} be the flow rate when $\sigma_j = +1$ and a^1_{ij} be that when $\sigma_j = -1$. We also define o^g_{ij} as the flow rate at which the cars on road (i, j) pass through the intersection i per unit time when the traffic light at the intersection i is green. Due to the presence of a dedicated right- or left-turn lane, vehicles may pass through the intersection j even when the traffic light is red. In this case, we define o^r_{ij} as the rate of such an outflow. A visualization of the definition of these flow rates is shown in Fig. 9. The value of a^0_{ij}, a^1_{ij}, o^g_{ij}, and o^r_{ij} may be known in advance, or they may be adaptively calculated by tracking the number of cars q_{ij} during traffic control. The calculation of these values in the present experiment is described later.

We can respectively calculate the flow rate at which cars enter and exit road (i, j) as

$$\frac{1}{2}a^0_{ij}(\sigma_j + 1) + \frac{1}{2}a^1_{ij}(-\sigma_j + 1) = \frac{1}{2}(\bar{a}_{ij} + a^\Delta_{ij}\sigma_j), \tag{14}$$

$$\frac{1}{2}o^g_{ij}(s_{ij}\sigma_i + 1) + \frac{1}{2}o^r_{ij}(-s_{ij}\sigma_i + 1) = \frac{1}{2}(\bar{o}^g_{ij} + o^\Delta_{ij}s_{ij}\sigma_i), \tag{15}$$

where we define $(\bar{a}_{ij}, a^\Delta_{ij}) = (a^0_{ij}+a^1_{ij}, a^0_{ij}-a^1_{ij})$ and $(\bar{o}_{ij}, o^\Delta_{ij}) = (o^g_{ij}+o^r_{ij}, o^g_{ij}-o^r_{ij})$. Then, the time evolution of the number of cars q_{ij} on the road (i, j) is

$$\frac{\mathrm{d}t}{\mathrm{d}q_{ij}} = \frac{1}{2}\bar{a}_{ij} + \frac{1}{2}a^\Delta_{ij}\sigma_j - \frac{1}{2}\bar{o}_{ij} - \frac{1}{2}o^\Delta_{ij}s_{ij}\sigma_i. \tag{16}$$

From Eq. (16) and Eq. (1), the time evolution of the vehicle bias x_i is calculated as follows:

$$\frac{\mathrm{d}t}{\mathrm{d}x_i} = \sum_{j\in N_i}\eta_{ij}s_{ij}(\bar{a}_{ij} + a^\Delta_{ij}\sigma_j - \bar{o}_{ij} - o^\Delta_{ij}s_{ij}\sigma_i). \tag{17}$$

Recall that we defined the vectors $x = [x_1, x_2, \ldots, x_N]^\top$ and $\sigma = [\sigma_1, \sigma_2, \ldots, \sigma_N]^\top$. We can rewrite Eq. (17) in vector form by using the matrix $A \in \mathbb{R}^{N\times N}$, which is defined as follows:

$$A_{ij} = \begin{cases} -\sum_{j\in N_i} \eta_{ij} o_{ij}^{\Delta} & i = j, \\ \eta_{ij} s_{ij} a_{ij}^{\Delta} & i \neq j,\ (i,j) \in E, \\ 0 & i \neq j,\ (i,j) \notin E. \end{cases} \tag{18}$$

We also define the vector $b = [b_1, b_2, \ldots, b_N]^\top \in \mathbb{R}^N$ as follows:

$$b_i = \sum_{j\in N_i} \eta_{ij} s_{ij} (\bar{a}_{ij} - \bar{o}_{ij}), \quad i = 1, \ldots, N. \tag{19}$$

Then, the time evolution in Eq. (17) is written as follows:

$$\frac{\mathrm{d}t}{\mathrm{d}x} = A\sigma + b. \tag{20}$$

We assumed that the traffic signal states $\sigma(t)$ do not change from time t to $t + \tau$ if the states are updated at time t. Therefore, we can integrate the above to obtain the following difference equation:

$$\begin{aligned} x(t+\tau) &= x(t) + (A\sigma(t) + b)\tau \\ &= x(t) + \tilde{A}\sigma(t) + \tilde{b}, \end{aligned} \tag{21}$$

where we defined $\tilde{A} = A\tau$ and $\tilde{b} = b\tau$.

CALCULATION OF WEIGHT PARAMETER IN VEHICLE BIAS

Here, we describe how we determine the coefficients $\eta_{ij} > 0$, which were introduced to define vehicle bias in Eq. (1). We consider the reference values for the length and number of cars on the road, denoted by L^{ref} and N^{ref}, respectively. We define the normalized density of cars on the road $\tilde{q}_{ij}$ as

$$\tilde{q}_{ij} = \frac{q_{ij}/N^{\mathrm{ref}}}{L_{ij}/L^{\mathrm{ref}}}, \tag{22}$$

where L_{ij} denotes the length of the road (j, i). According to our assumption, there are only four-way or three-way intersections. When intersection i is a four-way intersection, it holds that $s_{ij} = +1$ for two of the incoming roads and $s_{ij} = -1$ for the other two. Therefore, we can easily define the vehicle bias x_i by summing $s_{ij}\tilde{q}_{ij}$ over j. When intersection i is a three-way intersection, either $s_{ij} = +1$ or $s_{ij} = -1$ holds for only one incoming road. For intersections with such an imbalance, we define the bias of the number of vehicles x_i as follows:

$$x_i = 2\sum_{j\in\mathcal{N}_i} c_{ij}\tilde{q}_{ij}, \tag{23}$$

where the coefficient takes $c_{ij} = 2$ for the road (j, i) if there is no other road that leads to the same intersection i and has the same s_{ij}, and otherwise $c_{ij} = 1$. From the definition of $\tilde{q}_{ij}$, we obtain

$$x_i = 2\sum_{j\in\mathcal{N}_i} \frac{c_{ij}L^{\mathrm{ref}}}{N^{\mathrm{ref}}L_{ij}} q_{ij}, \tag{24}$$

which leads to the following definition of η_{ij}:

$$\eta_{ij} = \frac{c_{ij}L^{\mathrm{ref}}}{N^{\mathrm{ref}}L_{ij}}. \tag{25}$$

CALCULATION OF IN/OUT-FLOW VELOCITY

We describe how to determine the rates of inflow $a_{i,j}^s$ ($s \in \{0, 1\}$) and outflow $o_{i,j}^s$ ($s \in \{g, r\}$) for the road (i, j). These flow rates can be updated by counting each vehicle's travel path over a certain period while controlling the signals. Such online updates are effective in situations where traffic conditions change rapidly. In situations where rapid changes do not occur, it is sufficient to measure and fix these parameters in advance. In this study, we determined the parameters using the latter method.

First, consider the rate of inflow $a_{i,j}^s$ for $s = 0$. For road (j, k) leading to intersection j, when vehicles on the road exit, they will enter one of the roads starting from intersection j. Let p_{ijk} be the rate of vehicles entering the road (i, j). Then, the flow rate of vehicles entering the road (i, j) through intersection j from the road (j, k) can be estimated by multiplying the rate of vehicles exiting the road (j, k) by the probability p_{ijk} when intersection j is passable. Thus, when $s = 0$, we obtain

$$a_{ij}^0 = \sum_k o_{jk}^g p_{ijk}, \tag{26}$$

where the sum is taken over k such that the traffic signal in the state $\sigma_j = +1$ allows the cars to exit from road (j, k). In the case of $s = 1$, a_{ij}^1 is obtained by summing the same values over k such that the outflow is possible when $\sigma_j = -1$.

The rate of outflow o_{ij}^g can be calculated as N_{ij}^e/T_{ij}^g, where T_{ij}^g is the number of seconds when the traffic light indicates green for the road (i, j), and N_{ij}^e is the actual number of vehicles that leave the road. However, T_{ij}^g and N_{ij}^e take small values, especially in the transient state in the earlier period of the simulation, which makes the calculation unstable. Therefore, in our experiment, the rate of outflow is assumed to be the same for all roads and is calculated as follows:

$$o_{ij}^g = \frac{\sum_{(i,j)\in E} N_{ij}^e}{\sum_{(i,j)\in E} T_{ij}^g}. \tag{27}$$

Similarly, the rate of outflow o_{ij}^r may depend on the number of vehicles entering the intersection when the traffic light indicates red. However, it is always 0 unless there is a dedicated left/right turn lane on the road.

SIMULATOR IMPLEMENTATION DETAILS

All experiments in this study were conducted on a Linux computer with 64 GB of memory and a clock speed of 3.70 GHz.

In SUMO [62], states such as vehicle positions and speeds are updated sequentially at each time step (here, set to 1 second). All roads are implemented as left-side travel lanes. To obtain parameters for the Ising problem used by the controller, the simulator collects statistical information about

the traffic on the road network. The road network consists of roads with two lanes in opposite directions. Intersections are assumed to be three- or four-way intersections. In the implementation of the signal displays determined by AMPIC in SUMO, the behavior of real traffic signals is replicated. Specifically, when a signal changes from green to red in the direction of traffic flow, a yellow signal is displayed for 3 seconds, followed by a red signal for a further 3 seconds for both directions. The vehicles are generated at the originating intersection every p seconds in the simulation time (i.e., the vehicle generation rate is $1/p$) and the vehicles are removed from the simulator when they arrive at the destination. The origin and destination are located at intersections and are chosen independently at random with uniformly weighted probabilities. The route selection of each vehicle to its destination has a significant impact on overall traffic conditions [61]. Various methods have been developed for smarter route selection by autonomous driving and car navigation systems [104], [105], [106], [107]. In this study, we consider a scenario where each vehicle follows a basic route selection strategy, with routes generated using *duarouter* (https://sumo.dlr.de/docs/duarouter.html), a tool included in the SUMO tool set.

In AMPIC, the solvers provided by D-Wave Systems are used. Specifically, we use *greedy.SteepestDescentSolver* (https://docs.ocean.dwavesys.com/projects/greedy/en/latest/reference/samplers.html) for the greedy method, *SimulatedAnnealingSampler* (https://docs.ocean.dwavesys.com/projects/neal/en/latest/reference/sampler.html) for the simulated annealing method, and *DWaveSampler* (https://docs.ocean.dwavesys.com/projects/system/en/stable/reference/samplers.html) for the quantum annealing method. For the latter two methods, the parameter *num_reads* is set to 1 000. In the setting of QA, we use *EmbeddingComposite* (https://dwave-systemdocs.readthedocs.io/en/samplers/reference/composites/embedding.html) for the embeddings for the variables and use *Advantage_system5.4* for the solver.

Finally, the datasets analyzed in this study, as well as the code used to generate all the results, are available on GitHub, accessible at the following link: https://github.com/ToyotaCRDL/ampic.

ACKNOWLEDGMENT

The authors would like to thank Dr. Tadayoshi Matsumori and Dr. Norihiro Oyama of Toyota Central Research and Development Labs., Inc., for their useful discussions.

REFERENCES

[1] G. Weisbrod, D. Vary, and G. Treyz, "Measuring economic costs of urban traffic congestion to business," *Transp. Res. Rec. J. Transp. Res. Board*, vol. 1839, no. 1, pp. 98–106, Jan. 2003.

[2] J. I. Levy, J. J. Buonocore, and K. von Stackelberg, "Evaluation of the public health impacts of traffic congestion: A health risk assessment," *Environ. Health*, vol. 9, no. 1, p. 65, Oct. 2010.

[3] M. Barth and K. Boriboonsomsin, "Real-world carbon dioxide impacts of traffic congestion," *Transp. Res. Rec., J. Transp. Res. Board*, vol. 2058, no. 1, pp. 163–171, Jan. 2008.

[4] V. K. Arora et al., "Carbon-concentration and carbon-climate feedbacks in CMIP5 Earth system models," *J. Climate*, vol. 26, no. 15, pp. 5289–5314, Feb. 2013.

[5] M. R. Allen, D. J. Frame, C. Huntingford, C. D. Jones, J. A. Lowe, M. Meinshausen, and N. Meinshausen, "Warming caused by cumulative carbon emissions towards the trillionth tonne," *Nature*, vol. 458, no. 7242, pp. 1163–1166, Apr. 2009.

[6] *Climate Change 2021: The Physics Science Basis. Contribution Work. Group I To 6th Assessment Rep. Intergovernmental Panel Climate Change*. Cambridge, U.K.: Cambridge Univ. Press, 2021, pp. 3–32.

[7] S. S. S. M. Qadri, M. A. Gökçe, and E. Öner, "State-of-art review of traffic signal control methods: Challenges and opportunities," *Eur. Transp. Res. Rev.*, vol. 12, no. 1, p. 55, Oct. 2020.

[8] H. Wei, G. Zheng, V. Gayah, and Z. Li, "A survey on traffic signal control methods," 2020, *arXiv:1904.08117*.

[9] P. Diakaki, D. Kotsialos, and Wang, "Review of road traffic control strategies," *Proc. IEEE*, vol. 91, no. 12, pp. 2041–2042, Dec. 2003.

[10] A. J. Miller, "Settings for fixed-cycle traffic signals," *OR*, vol. 14, no. 4, p. 373, Dec. 1963.

[11] N. H. Gartner, "OPAC: A dmand-responsive strategy for traffic signal control," *Transp. Res. Rec.*, vol. 3, no. 906, pp. 1–26, 1983.

[12] D. Zhao, Y. Dai, and Z. Zhang, "Computational intelligence in urban traffic signal control: A survey," *IEEE Trans. Syst. Man, Cybern., Part C*, vol. 42, no. 4, pp. 485–494, Jul. 2012.

[13] Y. Wu and C. Ho, "The development of Taiwan arterial traffic-adaptive signal control system and its field test: A Taiwan experience," *J. Adv. Transp.*, vol. 43, no. 4, pp. 455–480, Oct. 2009.

[14] X. Cheng, L. Yang, and X. Shen, "D2D for intelligent transportation systems: A feasibility study," *IEEE Trans. Intell. Transp. Syst.*, vol. 16, no. 4, pp. 1784–1793, Aug. 2015.

[15] J. Zhang, F.-Y. Wang, K. Wang, W.-H. Lin, X. Xu, and C. Chen, "Data-driven intelligent transportation systems: A survey," *IEEE Trans. Intell. Transp. Syst.*, vol. 12, no. 4, pp. 1624–1639, Dec. 2011.

[16] N.-E.-E. Faouzi, H. Leung, and A. Kurian, "Data fusion in intelligent transportation systems: Progress and challenges—A survey," *Inf. Fusion*, vol. 12, no. 1, pp. 4–10, Jan. 2011.

[17] P. Mirchandani and L. Head, "A real-time traffic signal control system: Architecture, algorithms, and analysis," *Transp. Res. Part C, Emerg. Technol.*, vol. 9, no. 6, pp. 415–432, Dec. 2001.

[18] Y. Wang, X. Yang, H. Liang, and Y. Liu, "A review of the self-adaptive traffic signal control system based on future traffic environment," *J. Adv. Transp.*, vol. 2018, pp. 1–12, Jun. 2018.

[19] P. Jing, H. Huang, and L. Chen, "An adaptive traffic signal control in a connected vehicle environment: A systematic review," *Information*, vol. 8, no. 3, p. 101, Aug. 2017.

[20] S. Lin, B. De Schutter, Y. Xi, and H. Hellendoorn, "Fast model predictive control for urban road networks via MILP," *IEEE Trans. Intell. Transp. Syst.*, vol. 12, no. 3, pp. 846–856, Sep. 2011.

[21] Z. Li and P. Schonfeld, "Hybrid simulated annealing and genetic algorithm for optimizing arterial signal timings under oversaturated traffic conditions," *J. Adv. Transp.*, vol. 49, no. 1, pp. 153–170, Jan. 2015.

[22] Z. Li, M. Shahidehpour, S. Bahramirad, and A. Khodaei, "Optimizing traffic signal settings in smart cities," *IEEE Trans. Smart Grid*, vol. 8, no. 5, pp. 2382–2393, Sep. 2017.

[23] J. Guo, Y. Kong, Z. Li, W. Huang, J. Cao, and Y. Wei, "A model and genetic algorithm for area-wide intersection signal optimization under user equilibrium traffic," *Math. Comput. Simul.*, vol. 155, pp. 92–104, Jan. 2019.

[24] A. S. Akopov and L. A. Beklaryan, "Traffic improvement in Manhattan road networks with the use of parallel hybrid biobjective genetic algorithm," *IEEE Access*, vol. 12, pp. 19532–19552, 2024.

[25] H. S. E. Chuo, M. K. Tan, A. C. H. Chong, R. K. Y. Chin, and K. T. K. Teo, "Evolvable traffic signal control for intersection congestion alleviation with enhanced particle swarm optimisation," in *Proc. IEEE 2nd Int. Conf. Autom. Control Intell. Syst. (I2CACIS)*, Oct. 2017, pp. 92–97.

[26] S. S. Leal, P. E. M. de Almeida, and E. Chung, "Active control for traffic lights in regions and corridors: An approach based on evolutionary computation," *Transp. Res. Proc.*, vol. 25, pp. 1769–1780, Jan. 2017.

[27] M. Bernas, B. Płaczek, and J. Smyla, "A neuroevolutionary approach to controlling traffic signals based on data from sensor network," *Sensors*, vol. 19, no. 8, p. 1776, Apr. 2019.

[28] S. Araghi, A. Khosravi, D. Creighton, and S. Nahavandi, "Influence of meta-heuristic optimization on the performance of adaptive interval type2-fuzzy traffic signal controllers," *Expert Syst. Appl.*, vol. 71, pp. 493–503, Apr. 2017.
[29] M. D. Simoni and C. G. Claudel, "A semi-analytic approach to model signal plans in urban corridors and its application in Metaheuristic optimization," *Transportmetrica B, Transp. Dyn.*, vol. 7, no. 1, pp. 185–201, Dec. 2019.
[30] K. Gao, Y. Zhang, R. Su, F. Yang, P. N. Suganthan, and M. Zhou, "Solving traffic signal scheduling problems in heterogeneous traffic network by using meta-heuristics," *IEEE Trans. Intell. Transp. Syst.*, vol. 20, no. 9, pp. 3272–3282, Sep. 2019.
[31] F. Rasheed, K. A. Yau, R. Md. Noor, C. Wu, and Y.-C. Low, "Deep reinforcement learning for traffic signal control: A review," *IEEE Access*, vol. 8, pp. 208016–208044, 2020.
[32] M. Gregurić, M. Vujić, C. Alexopoulos, and M. Miletić, "Application of deep reinforcement learning in traffic signal control: An overview and impact of open traffic data," *Appl. Sci.*, vol. 10, no. 11, p. 4011, Jun. 2020.
[33] T. Nishi, K. Otaki, K. Hayakawa, and T. Yoshimura, "Traffic signal control based on reinforcement learning with graph convolutional neural nets," in *Proc. 21st Int. Conf. Intell. Transp. Syst. (ITSC)*, Nov. 2018, pp. 877–883.
[34] C. Ozan, O. Baskan, S. Haldenbilen, and H. Ceylan, "A modified reinforcement learning algorithm for solving coordinated signalized networks," *Transp. Res. Part C, Emerg. Technol.*, vol. 54, pp. 40–55, May 2015.
[35] X. Liang, X. Du, G. Wang, and Z. Han, "A deep reinforcement learning network for traffic light cycle control," *IEEE Trans. Veh. Technol.*, vol. 68, no. 2, pp. 1243–1253, Feb. 2019.
[36] G. S. van de Weg, H. L. Vu, A. Hegyi, and S. P. Hoogendoorn, "A hierarchical control framework for coordination of intersection signal timings in all traffic regimes," *IEEE Trans. Intell. Transp. Syst.*, vol. 20, no. 5, pp. 1815–1827, May 2019.
[37] R. Mohebifard and A. Hajbabaie, "Optimal network-level traffic signal control: A benders decomposition-based solution algorithm," *Transp. Res. Part B, Methodol.*, vol. 121, pp. 252–274, Mar. 2019.
[38] P. Varaiya, "Max pressure control of a network of signalized intersections," *Transp. Res. Part C, Emerg. Technol.*, vol. 36, pp. 177–195, Nov. 2013.
[39] S. Choi, B. B. Park, J. Lee, H. Lee, and S. H. Son, "Field implementation feasibility study of cumulative travel-time responsive (CTR) traffic signal control algorithm," *J. Adv. Transp.*, vol. 50, no. 8, pp. 2226–2238, Dec. 2016.
[40] C. N. Yang, "The spontaneous magnetization of a two-dimensional ising model," *Phys. Rev.*, vol. 85, no. 5, pp. 808–816, Mar. 1952.
[41] B. M. McCoy and T. T. Wu, *The Two-Dimensional Ising Model*. Harvard Univ. Press, 2013.
[42] F. Glover, G. Kochenberger, and Y. Du, "Applications and computational advances for solving the QUBO model," in *The Quadratic Unconstrained Binary Optimization Problem*. Springer, 2022, pp. 39–56.
[43] F. Glover, G. Kochenberger, and Y. Du, "A tutorial on formulating and using QUBO models," 2018, *arXiv:1811.11538*.
[44] M. W. Johnson et al., "Quantum annealing with manufactured spins," *Nature*, vol. 473, no. 7346, pp. 194–198, May 2011.
[45] H. Goto, K. Tatsumura, and A. R. Dixon, "Combinatorial optimization by simulating adiabatic bifurcations in nonlinear Hamiltonian systems," *Sci. Adv.*, vol. 5, no. 4, p. 2372, Apr. 2019.
[46] R. Hamerly et al., "Experimental investigation of performance differences between coherent ising machines and a quantum annealer," *Sci. Adv.*, vol. 5, no. 5, pp. 1–20, May 2019.
[47] F. Neukart, G. Compostella, C. Seidel, D. von Dollen, S. Yarkoni, and B. Parney, "Traffic flow optimization using a quantum annealer," *Frontiers ICT*, vol. 4, pp. 1–18, Dec. 2017.
[48] T. Stollenwerk, B. O'Gorman, D. Venturelli, S. Mandra, O. Rodionova, H. Ng, B. Sridhar, E. G. Rieffel, and R. Biswas, "Quantum annealing applied to de-conflicting optimal trajectories for air traffic management," *IEEE Trans. Intell. Transp. Syst.*, vol. 21, no. 1, pp. 285–297, Jan. 2020.
[49] D. Inoue and H. Yoshida, "Model predictive control for finite input systems using the D-Wave quantum annealer," *Sci. Rep.*, vol. 10, no. 1, pp. 1–10, Jan. 2020.
[50] K. Otaki, A. Okada, and H. Yoshida, "Experimental study on the information disclosure problem: Branch-and-bound and QUBO solver," *Frontiers Appl. Math. Statist.*, vol. 9, pp. 1–19, Mar. 2023.
[51] A. Okada, H. Yoshida, K. Kidono, T. Matsumori, T. Takeno, and T. Kadowaki, "Design optimization of noise filter using quantum annealer," *IEEE Access*, vol. 11, pp. 44343–44349, 2023.
[52] K. Terada, D. Oku, S. Kanamaru, S. Tanaka, M. Hayashi, M. Yamaoka, M. Yanagisawa, and N. Togawa, "An ising model mapping to solve rectangle packing problem," in *Proc. Int. Symp. VLSI Design, Autom. Test (VLSI-DAT)*, Apr. 2018, pp. 1–4.
[53] M. Ohzeki, A. Miki, M. J. Miyama, and M. Terabe, "Control of automated guided vehicles without collision by quantum annealer and digital devices," *Frontiers Comput. Sci.*, vol. 1, pp. 1–23, Nov. 2019.
[54] Z. I. Tabi, Á. Marosits, Z. Kallus, P. Vaderna, I. Gódor, and Z. Zimborás, "Evaluation of quantum annealer performance via the massive MIMO problem," *IEEE Access*, vol. 9, pp. 131658–131671, 2021.
[55] S. Yarkoni, A. Alekseyenko, M. Streif, D. Von Dollen, F. Neukart, and T. Bäck, "Multi-car paint shop optimization with quantum annealing," in *Proc. IEEE Int. Conf. Quantum Comput. Eng. (QCE)*, Oct. 2021, pp. 35–41.
[56] D. Inoue, A. Okada, T. Matsumori, K. Aihara, and H. Yoshida, "Traffic signal optimization on a square lattice with quantum annealing," *Sci. Rep.*, vol. 11, no. 1, p. 3303, Feb. 2021.
[57] H. Hussain, M. B. Javaid, F. S. Khan, A. Dalal, and A. Khalique, "Optimal control of traffic signals using quantum annealing," *Quantum Inf. Process.*, vol. 19, no. 9, p. 312, Aug. 2020.
[58] A. Marchesin, B. Montrucchio, M. Graziano, A. Boella, and G. Mondo, "Improving urban traffic mobility via a versatile quantum annealing model," *IEEE Trans. Quantum Eng.*, vol. 4, pp. 1–13, 2023.
[59] R. Shikanai, M. Ohzeki, and K. Tanaka, "Traffic signal optimization using quantum annealing on real map," 2023, *arXiv:2308.14462*.
[60] B.-L. Ye, W. Wu, K. Ruan, L. Li, T. Chen, H. Gao, and Y. Chen, "A survey of model predictive control methods for traffic signal control," *IEEE/CAA J. Automatica Sinica*, vol. 6, no. 3, pp. 623–640, May 2019.
[61] Q. Guo, L. Li, and X. J. Ban, "Urban traffic signal control with connected and automated vehicles: A survey," *Transp. Res. Part C, Emerg. Technol.*, vol. 101, pp. 313–334, Apr. 2019.
[62] P. A. Lopez, M. Behrisch, L. Bieker-Walz, J. Erdmann, Y.-P. Flötteröd, R. Hilbrich, L. Lucken, J. Rummel, P. Wagner, and E. Wiessner, "Microscopic traffic simulation using SUMO," in *Proc. 21st Int. Conf. Intell. Transp. Syst. (ITSC)*, Nov. 2018, pp. 2575–2582.
[63] L. B. de Oliveira and E. Camponogara, "Predictive control for urban traffic networks: Initial evaluation," *IFAC Proc. Volumes*, vol. 40, no. 20, pp. 424–429, 2007.
[64] K. Aboudolas, M. Papageorgiou, A. Kouvelas, and E. Kosmatopoulos, "A rolling-horizon quadratic-programming approach to the signal control problem in large-scale congested urban road networks," *Transp. Res. Part C, Emerg. Technol.*, vol. 18, no. 5, pp. 680–694, Oct. 2010.
[65] B. De Schutter, H. Hellendoorn, A. Hegyi, M. van den Berg, and S. K. Zegeye, "Model-based control of intelligent traffic networks," in *Intelligent Infrastructures*. Cham, Switzerland: Springer, 2010, pp. 277–310.
[66] B.-L. Ye, W. Wu, L. Li, and W. Mao, "A hierarchical model predictive control approach for signal splits optimization in large-scale urban road networks," *IEEE Trans. Intell. Transp. Syst.*, vol. 17, no. 8, pp. 2182–2192, Aug. 2016.
[67] Z. Zhou, B. De Schutter, S. Lin, and Y. Xi, "Two-level hierarchical model-based predictive control for large-scale urban traffic networks," *IEEE Trans. Control Syst. Technol.*, vol. 25, no. 2, pp. 496–508, Mar. 2017.
[68] F. A. de Souza, V. B. Peccin, and E. Camponogara, "Distributed model predictive control applied to urban traffic networks: Implementation, experimentation, and analysis," in *Proc. IEEE Int. Conf. Autom. Sci. Eng.*, Aug. 2010, pp. 399–405.
[69] E. Camponogara and H. F. Scherer, "Distributed optimization for model predictive control of linear dynamic networks with control-input and output constraints," *IEEE Trans. Autom. Sci. Eng.*, vol. 8, no. 1, pp. 233–242, Jan. 2011.
[70] F. A. de Souza, E. Camponogara, W. Kraus, and V. B. Peccin, "Distributed MPC for urban traffic networks: A simulation-based performance analysis," *Optim. Control Appl. Methods*, vol. 36, no. 3, pp. 353–368, May 2015.
[71] B. Ye, W. Wu, and W. Mao, "Distributed model predictive control method for optimal coordination of signal splits in urban traffic networks," *Asian J. Control*, vol. 17, no. 3, pp. 775–790, May 2015.

[72] I. A. Villalobos, A. S. Poznyak, and A. M. Tamayo, "Urban traffic control problem: A game theory approach," *IFAC Proc. Volumes*, vol. 41, no. 2, pp. 7154–7159, 2008.

[73] P. G. Balaji, X. German, and D. Srinivasan, "Urban traffic signal control using reinforcement learning agents," *IET Intell. Transp. Syst.*, vol. 4, no. 3, pp. 177–188, Sep. 2010.

[74] D. McKenney and T. White, "Distributed and adaptive traffic signal control within a realistic traffic simulation," *Eng. Appl. Artif. Intell.*, vol. 26, no. 1, pp. 574–583, Jan. 2013.

[75] M. Xu, K. An, L. H. Vu, Z. Ye, J. Feng, and E. Chen, "Optimizing multi-agent based urban traffic signal control system," *J. Intell. Transp. Syst.*, vol. 23, no. 4, pp. 357–369, Jul. 2019.

[76] H. Abdelgawad, B. Abdulhai, S. El-Tantawy, A. Hadayeghi, and B. Zvaniga, "Assessment of self-learning adaptive traffic signal control on congested urban areas: Independent versus coordinated perspectives," *Can. J. Civil Eng.*, vol. 42, no. 6, pp. 353–366, Jun. 2015.

[77] Y. Feng, K. L. Head, S. Khoshmagham, and M. Zamanipour, "A real-time adaptive signal control in a connected vehicle environment," *Transp. Res. Part C, Emerg. Technol.*, vol. 55, pp. 460–473, Jun. 2015.

[78] J. Rios-Torres and A. A. Malikopoulos, "A survey on the coordination of connected and automated vehicles at intersections and merging at highway on-ramps," *IEEE Trans. Intell. Transp. Syst.*, vol. 18, no. 5, pp. 1066–1077, May 2017.

[79] J. Guanetti, Y. Kim, and F. Borrelli, "Control of connected and automated vehicles: State of the art and future challenges," *Annu. Rev. Control*, vol. 45, pp. 18–40, Apr. 2018.

[80] H. Qi, R. Dai, Q. Tang, and X. Hu, "Coordinated intersection signal design for mixed traffic flow of human-driven and connected and autonomous vehicles," *IEEE Access*, vol. 8, pp. 26067–26084, 2020.

[81] M. Eom and B.-I. Kim, "The traffic signal control problem for intersections: A review," *Eur. Transp. Res. Rev.*, vol. 12, no. 1, p. 50, Sep. 2020.

[82] J. Li, C. Yu, Z. Shen, Z. Su, and W. Ma, "A survey on urban traffic control under mixed traffic environment with connected automated vehicles," *Transp. Res. Part C, Emerg. Technol.*, vol. 154, Sep. 2023, Art. no. 104258.

[83] T. Inagaki, Y. Haribara, K. Igarashi, T. Sonobe, S. Tamate, T. Honjo, A. Marandi, P. L. Mcmahon, T. Umeki, K. Enbutsu, O. Tadanaga, H. Takenouchi, K. Aihara, K.-I. Kawarabayashi, K. Inoue, S. Utsunomiya, and H. Takesue, "A coherent ising machine for 2000-node optimization problems," *Science*, vol. 354, no. 6312, pp. 603–606, Nov. 2016.

[84] S. Matsubara, H. Tamura, M. Takatsu, D. Yoo, B. Vatankhahghadim, H. Yamasaki, T. Miyazawa, S. Tsukamoto, Y. Watanabe, K. Takemoto, and A. Sheikholeslami, "Ising-model optimizer with parallel-trial bit-sieve engine," in *Complex, Intelligent, and Software Intensive Systems*. Cham, Switzerland: Springer, 2018, pp. 432–438.

[85] M. Aramon, G. Rosenberg, E. Valiante, T. Miyazawa, H. Tamura, and H. G. Katzgraber, "Physics-inspired optimization for quadratic unconstrained problems using a digital annealer," *Frontiers Phys.*, vol. 7, pp. 1–20, Apr. 2019.

[86] T. Kadowaki and H. Nishimori, "Quantum annealing in the transverse ising model," *Phys. Rev. E, Stat. Phys. Plasmas Fluids Relat. Interdiscip. Top.*, vol. 58, no. 5, pp. 5355–5363, Nov. 1998.

[87] J. King, S. Yarkoni, M. M. Nevisi, J. P. Hilton, and C. C. McGeoch, "Benchmarking a quantum annealing processor with the time-to-target metric," 2015, *arXiv:1508.05087*.

[88] C. C. McGeoch and C. Wang, "Experimental evaluation of an adiabatic quantum system for combinatorial optimization," in *Proc. ACM Int. Conf. Comput. Frontiers*, May 2013, p. 23.

[89] D. Venturelli, D. J. J. Marchand, and G. Rojo, "Quantum annealing implementation of job-shop scheduling," 2015, *arXiv:1506.08479*.

[90] D. O'Malley, V. V. Vesselinov, B. S. Alexandrov, and L. B. Alexandrov, "Nonnegative/Binary matrix factorization with a D-Wave quantum annealer," *PLoS ONE*, vol. 13, no. 12, Dec. 2018, Art. no. e0206653.

[91] M. Ohzeki, S. Okada, M. Terabe, and S. Taguchi, "Optimization of neural networks via finite-value quantum fluctuations," *Sci. Rep.*, vol. 8, no. 1, pp. 1–10, Jul. 2018.

[92] R. Ayanzadeh, M. Halem, and T. Finin, "Reinforcement quantum annealing: A hybrid quantum learning automata," *Sci. Rep.*, vol. 10, no. 1, p. 7952, May 2020.

[93] D. Krajzewicz, M. Behrisch, P. Wagner, R. Luz, and M. Krumnow, "Second generation of pollutant emission models for SUMO," in *Proc. 2nd SUMO Conf.*, 2014, pp. 203–221.

[94] H. Suzuki, J.-I. Imura, and K. Aihara, "Chaotic ising-like dynamics in traffic signals," *Sci. Rep.*, vol. 3, no. 1, pp. 1–6, Jan. 2013.

[95] *Simulated Annealing Sampler documentation*. Accessed: Dec. 1, 2024. [Online]. Available: https://docs.ocean.dwavesys.com/projects/neal/en/latest/reference/sampler.html

[96] *Openstreetmap*. Accessed: Dec. 1, 2024. [Online]. Available: https://www.openstreetmap.org/copyright

[97] M. Haklay and P. Weber, "OpenStreetMap: User-generated street maps," *IEEE Pervasive Comput.*, vol. 7, no. 4, pp. 12–18, Oct. 2008.

[98] *Map: Map in English Based on OpenStreetMap Data*. Accessed: Dec. 1, 2024. [Online]. Available: https://www.osmap.us

[99] *Operation and Timing—D-Wave System Documentation*. Accessed: Dec. 1, 2024. [Online]. Available: https://docs.dwavesys.com/docs/latest/c_qpu_timing.html

[100] H. Oshiyama and M. Ohzeki, "Benchmark of quantum-inspired heuristic solvers for quadratic unconstrained binary optimization," *Sci. Rep.*, vol. 12, no. 1, p. 2146, Feb. 2022.

[101] J.-R. Jiang and C.-W. Chu, "Classifying and benchmarking quantum annealing algorithms based on quadratic unconstrained binary optimization for solving NP-hard problems," *IEEE Access*, vol. 11, pp. 104165–104178, 2023.

[102] W.-C. Feng and K. Cameron, "The Green500 list: Encouraging sustainable supercomputing," *Computer*, vol. 40, no. 12, pp. 50–55, Dec. 2007.

[103] M. Yamaoka, C. Yoshimura, M. Hayashi, T. Okuyama, H. Aoki, and H. Mizuno, "A 20k-spin ising chip to solve combinatorial optimization problems with CMOS annealing," *IEEE J. Solid-State Circuits*, vol. 51, no. 1, pp. 303–309, Jan. 2016.

[104] D. González, J. Pérez, V. Milanés, and F. Nashashibi, "A review of motion planning techniques for automated vehicles," *IEEE Trans. Intell. Transp. Syst.*, vol. 17, no. 4, pp. 1135–1145, Apr. 2016.

[105] H. Bast, D. Delling, A. Goldberg, M. Müller-Hannemann, T. Pajor, P. Sanders, D. Wagner, and R. F. Werneck, "Route planning in transportation networks," in *Algorithm Engineering: Selected Results and Surveys*. Springer, 2016, pp. 19–80.

[106] J. Li, P. Surynek, A. Felner, H. Ma, T. K. Kumar, and S. Koenig, "Multi-agent path finding for large agents," *Proc. Int. Symp. Combinat. Search*, vol. 10, no. 1, pp. 186–187, Sep. 2021.

[107] S. Kumar and S. C. Sharma, "Optimal coverage path planning in a wireless sensor network for intelligent transportation system," *Int. J. Comput. Netw. Commun.*, vol. 15, no. 5, pp. 55–72, Sep. 2023.

DAISUKE INOUE received the B.E. degree in engineering from Osaka University, in 2014, the M.S. degree in informatics from Kyoto University, in 2017, and the Ph.D. degree in mathematical science from The University of Tokyo, in 2024. Since 2017, he has been with Toyota Central Research and Development Labs., Inc. His research interests include control of multi-agent systems and numerical computation of partial differential equations.

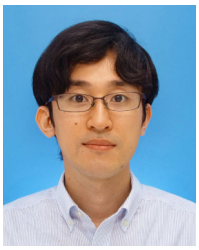

HIROSHI YAMASHITA received the B.E., M.I.S.T., and Ph.D. degrees in information science and technology from The University of Tokyo, in 2015, 2017, and 2020, respectively. He is currently an Assistant Professor with the Graduate School of Information Science and Technology, Osaka University. His research interests include computational methods for complex systems and their applications to data science and artificial intelligence.

KAZUYUKI AIHARA received the B.E. degree in electrical engineering and the Ph.D. degree in electronic engineering from The University of Tokyo (UTokyo), Tokyo, Japan, in 1977 and 1982, respectively. He is currently the University Professor and a Professor Emeritus with UTokyo, and the Executive Director of the International Research Center for Neurointelligence (IRCN), UTokyo. He has been studying mathematical theory for modelling complex systems in general and its transdisciplinary applications in science and technology from the viewpoint of mathematical engineering and chaos engineering.

HIROAKI YOSHIDA received the B.Eng., M.Eng., and Dr.-Eng. degrees from Kyoto University, in 2003, 2005, and 2007, respectively. He joined Toyota Central Research and Development Labs., Inc., in 2007, and his current position is the Leader of the Applied Mathematics Research Domain. From 2015 to 2017, he was a Visiting Researcher with École Normale Supérieure, Paris. His research interests include computational physics and micro-and nano-fluidics.